Design, implementation and study of the high-resolution high-efficiency liquid crystal on Silicon spatial light modulator for the telecommunication application in the short wave infrared spectral band

Po-Ju Chen[a,b*], Philip Engel[a], Grigory Lazarev[a], Adam Mazur[a], and H. Paul Urbach[b]

[a]HOLOEYE Photonics AG, Volmerstr. 1, 12489 Berlin, Germany
[b]Optics Research Group, Delft University of Technology, Lorentzweg 1, 2628 CJ Delft, The Netherlands

ABSTRACT

There are many important applications for phase-only liquid crystal on Silicon-based spatial light modulators (LCOS SLMs). Among the applications, the diffractive beam splitting, beam shaping and beam steering with LCOS SLM are finding more and more use in telecommunication applications (e.g. wavelength selective switch for ROADM, space and mode division multiplexing). However, many effects of LCOS device have to be considered if we want to get high quality output light field. For example, the ideal phase, intensity and polarization distribution in far field are usually deteriorated by the pixelated metal structure and fringing field effects. Thus, the total efficiency is decreased. By using electro-optical and electromagnetic simulation methods, we can properly incorporate the effects that influence the optical performance of LCOS and optimize the design. Furthermore we report the implementation of the high-performance high-resolution LCOS SLM for the telecommunication C- and L-band with the average insertion loss (IL) of less than 0.2 dB, achieved by the reflectivity-enhancement coating on the LCOS backplane. The experimental results on reflectivity, diffraction efficiency, crosstalk and other important parameters are compared with the theoretical predictions.

Keywords: Liquid Crystal on Silicon, Spatial light modulator, LCOS, beam steering, diffractive optics

1. INTRODUCTION

Liquid crystal on Silicon (LCOS) device is an electro-optical device that functions as dynamic spatial light modulator. Nowadays, LCOS has wide applications for diffraction-related technology, such as laser material processing,[1] beam shaping,[2] or beam steering.[3] For telecommunication-related application, reconfigurability and ability to do multilevel phase manipulation are the major advantages of LCOS. Generally speaking, LCOS is often used as a central part for mode converter[4,5] or wavelength selective switch[6–8] (WSS) in the telecommunication application. For former case, different phase masks were displayed on the LCOS to alternate the optical property of incident light with orthogonal spatial or polarization modes, which is a key component in space and mode division multiplexing. In wavelength-division multiplexing (WDM), a hologram or blazed gratings with different periods were displayed on different regions of LCOS panel to redirect the incoming light that consist of multiple wavelength into different output fibers.

Over last few years, LCOS started to play an important role for WSS in industrial reconfigurable optical add-drop multiplexer[8–10] (ROADM) to provide a flexible and reconfigurable routing in the complex and high capacity network architecture. For this application, the flicker, crosstalk and insertion loss (IL) induced by LCOS are three existing issues that can be improved to enhance the overall system performance. For crosstalk issue or the fringing field effect, which is the lateral electric field between neighboring pixels will create extra rotation or twist of liquid crystal (LC) molecules and affect the desired phase modulation depth. The phase flicker or the phase instability of LCOS over time is induced by the digital driving scheme as liquid crystal (LC) molecules response to the pulse signal over time. The IL, which indicates the loss between input fiber and output fiber,

Email: po-ju.chen@holoeye.com / p.chen-4@tudelft.nl

is affected by the fringing field effect and the reflectance of LCOS. As for the loss from reflectance of LCOS, it comes from the absorption of LC material, pixelated metallic structure on the backplane, and interference effects from the multiple reflections in the layers. Thus, to implement the high efficiency and high resolution LCOS for telecommunication applications, its important to reduce the flicker and the IL in the design process.

In this paper, we studied the optical properties of LCOS with high reflectance coating (HRC) layer along with digital driving scheme. The HRC layer was deposited between the alignment layer and the backplane, whereas normally the structure of reflective type LCOS only contains, from top to bottom, glass substrate, indium tin oxide (ITO), alignment layer, LC layer, alignment layer and backplane, as shown in Fig. 1. To further enhance the reflection, an index match layer and antireflection coating layer were coated on back and front sides of the glass substrate, which is not shown in Fig. 1. First, we perform the optical simulation and experiment for the LCOS in C-band (1530 nm∼1565 nm) and L-band (1565 nm∼1625 nm) before assembling and after assembling. Then, we investigate the phase stability of the LCOS for C-band. After the phase linearization, we display binary grating and blazed grating on LCOS and measure the diffraction efficiency for telecommunication waveband.

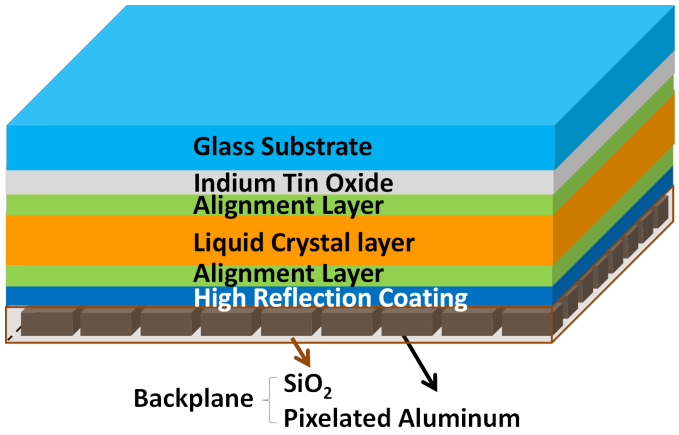

Figure 1. FEM simulation and experiment results for the backplane with and without HRC layer.

2. DESIGN AND IMPLEMENTATION OF THE LCOS DEVICE

2.1 Simulation and experiment results for LCOS Backplane with HRC layer

Here, we describe the design principle of HRC layer. Then we perform the finite element method (FEM) simulation by using JCMsuite software to compare the optical performance with and without the HRC layer on the LCOS Backplane. Finally, we compare simulation results with the experiment results. The design principle is to first choose the proper coating materials for telecommunication band application. The main consideration is that the materials should have lowest absorption in C- and L- band. Besides, the dielectric property of HRC layer should have minimized influence on the electrical field, applied between the ITO layer and the backplane. The HRC layer is using stack of dielectric materials. The HRC layer should be thin enough to maintain the feasible driving voltage across the LC layer. For preliminary parameters test and design, we assume 1D geometry variation on the backplane, for example pixelated Aluminum (Al) was treated as a grating structure. Based on fast 1D RCWA simulation[1,11] we can verify the combinations of several different materials as HRC layer and which combination can have thinnest layers.

Then, another rigorous simulation method, FEM, is used to simulate the optical performance and compare with the experiment results in 3D. In the simulation, we assume normal incidence of S and P polarization for wavelength changing from 1520 nm to 1580 nm with the step of 0.5 nm. We apply mirror symmetry boundary conditions on the backplane, where the pixel period and the interpixel gap are 8um and 300 nm respectively (corresponding to fill factor of 92.6 %), to speed up the simulation process. The degree of freedom of FEM simulation was adjusted to 3 to obtain higher accuracy.[12] The simulation results for the backplane with and

without HRC layer are shown in Fig. 2 as solid line and dash line, respectively. As for the line color, blue and red represent S and P polarization. Here, we can see that the reflectance of the backplane has improved from ∼93 % (0.315 dB) to ∼99 % (0.044 dB). The simulation results for S and P are identical to each other, which is as expected for normal incidence. We also observed resonance dip around 1538 nm for S and P polarization with HRC layer, which didnt show up in the simulation without HRC layer.

Finally, we measure the reflectance of the backplane with HRC layer from the wafer. In the experiment, the tunable laser with the tuning range 1520 nm to 1580 nm and the linewidth of 10kHz (CBDX1-1-HC1-FA, IDPHOTONICS) was used as a light source, and then a polarizer was put in front of the light source to keep it as P polarized incident light. Then, a beam splitter is put behind polarizer to separate the reflected light and incident light to monitor the fluctuation of the laser power during the measurement. Wafer sample or a gold mirror (M01, Thorlabs) was then put behind the beam splitter. Finally, two power meters (S132C, Thorlabs) were put separately in the opposite side of beam splitter to detect the optical power of reflected light and incident light. The reflectance of LCOS is thus first measured relative to that of the gold mirror. Then, it is multiplied with the reflectance data of the gold mirror to get the absolute values. The experiment results are the green solid line and dash line for the wafer with HRC layer and without HRC layer, as shown in Fig. 2. We have observed similar resonance dips around 1550 nm and 1554 nm, which locations differ from the simulation (1538 nm). The existence of resonance dip might be explained by the surface mode caused by pixelated structure, where HRC layer enhance the mode so it is only observed when the HRC layer was presented. The reasons for the double dips and the spectral shift might be due to the 5 degree tilt angle of the wafer during the measurement and the asymmetry of the underlining pixel structure, which creates differences for S and P polarizations. This can be e.g. related to non-symmetrical interpixel gap along two directions, i.e. 285 nm in one direction and 290 nm in another direction (instead of 300 nm in both). This question requires further verification with structure analysis using e.g. focused ion beam measurement. In conclusion, the HRC layer that deposited on the backplane has pretty good performance in C- and L-band, where the reflectance is over 95.5 % (IL smaller than 0.2dB) and better than that without HRC layer (86 % ∼ 88 %) .Only part of L-band could be verified experimentally, because of the spectral range limitation of the light source.

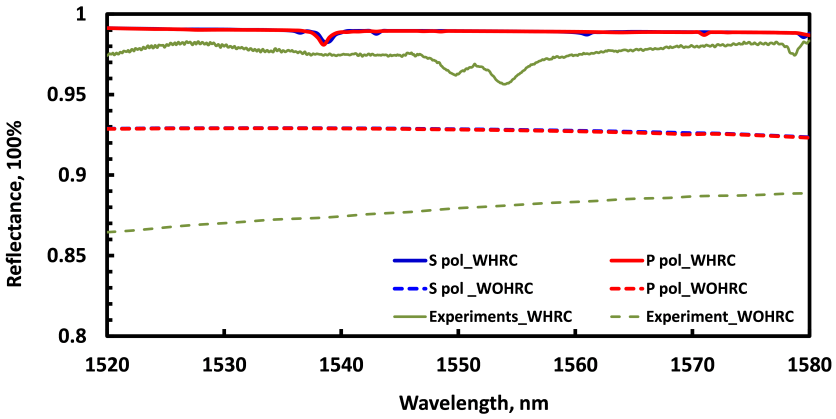

Figure 2. FEM simulation and experiment results for the backplane with and without HRC layer

2.2 Simulation and experiment results for the LCOS panel without applying voltage

To simulate the optical performance of the whole LCOS with the HRC layer, we use the combination of FEM method and transfer matrix method (TMM).[13] This is due to the fact that the thickness of the glass substrate (∼mm) is much larger compared to other parts of LCOS. Originally, we would aim to complete the 3D simulation, however, due to the fine metallic pixelated structure in the backplane and multiscale layers (∼nm to ∼mm) it became difficult. To get accurate simulation results means a lot of mesh points have to be incorporated in the simulation, which is hard to accomplish without large computation resources. As a result, to facilitate the

simulation process, we use 2D FEM simulation together with TMM method in the following prediction. The complex amplitude of the electric field for the zero order (reflection) was calculated using 2D FEM along the boundary of the bottom alignment layer, which is after the HRC layer. Then, we assume the incident E field (E_1^+) and the reflected E field (E_1^-) as unknown on the top glass substrate (layer 1). As for the output E field, which is the known incident field (E'^+_{M+1}) and reflected E field (E'^-_{M+1}) on the boundary between the LC layer (layer M) and the alignment layer (layer M+1), is pre-calculated by FEM methods. Then, we substitute the corresponding refraction matrix $D_{1,2}, \cdots, D_{M,M+1}$ at the each interface and the propagation matrix P_2, ., P_M inside each layer in Eq. 1, where $r_{1,2}, \cdots, r_{M,M+1}$ is the reflection coefficient and $t_{1,2}, \cdots, t_{M,M+1}$ is the transmission coefficient for each interface. And δ is the optical phase inside each layer, where n is the refractive index, d is the thickness and λ is the wavelength in vacuum. So finally the reflectance between bottom alignment layer and the glass substrate can be calculated using TMM method.

$$\begin{aligned}\begin{pmatrix} E_1^+ \\ E_1^- \end{pmatrix} &= D_{1,2}P_2D_{2,3}\cdots D_{M,M+1}\begin{pmatrix} E'^+_{M+1} \\ E'^-_{M+1} \end{pmatrix} \\ &= \begin{pmatrix} \frac{1}{t_{1,2}} & \frac{r_{1,2}}{t_{1,2}} \\ \frac{r_{1,2}}{t_{1,2}} & \frac{1}{t_{1,2}} \end{pmatrix}\begin{pmatrix} e^{i\delta_2} & 0 \\ 0 & e^{-i\delta_2} \end{pmatrix}\begin{pmatrix} \frac{1}{t_{2,3}} & \frac{r_{2,3}}{t_{2,3}} \\ \frac{r_{2,3}}{t_{2,3}} & \frac{1}{t_{2,3}} \end{pmatrix}\cdots\begin{pmatrix} \frac{1}{t_{M,M+1}} & \frac{r_{M,M+1}}{t_{M,M+1}} \\ \frac{r_{M,M+1}}{t_{M,M+1}} & \frac{1}{t_{M,M+1}} \end{pmatrix}\begin{pmatrix} E'^+_{M+1} \\ E'^+_{M+1} \end{pmatrix} \end{aligned} \quad (1)$$

The simulation results are shown in Fig. 3. The red and blue lines are the simulation results, which correspond to the LC medium with and without absorption taken into account respectively. Finally, we measure the reflectance of the LCOS without applying any voltage. The experiment set-up is the same as for the measurement of the backplane reflectance. The experiment results of the LCOS panel are shown as green line in Fig. 3. We observed the maximum reflectance of experiment result is around 96.7 % at 1549 nm and descend toward 93 % when wavelength shift toward 1520 nm and 1580 nm respectively. The high frequency oscillation is caused by the multiple beam interference effect for the reflections from the front surface of the cover glass and the HRC, the low frequency component is caused by the similar effect between HRC and the back surface of cover glass or ITO layer. As for the simulation results, we can see there is a region of high reflectance (∼97% and ∼99 % for the LC medium with and without absorption), which is around 1546 nm. We also found that the location of the peak reflectance area is dependent on the thickness of the LC layer, which is slightly varying spatially across the panel. The amplitude of the high-frequency oscillation in the experiment, compared with simulation results, might be reduced due to the surface roughness and thus additional scattering in the layers.

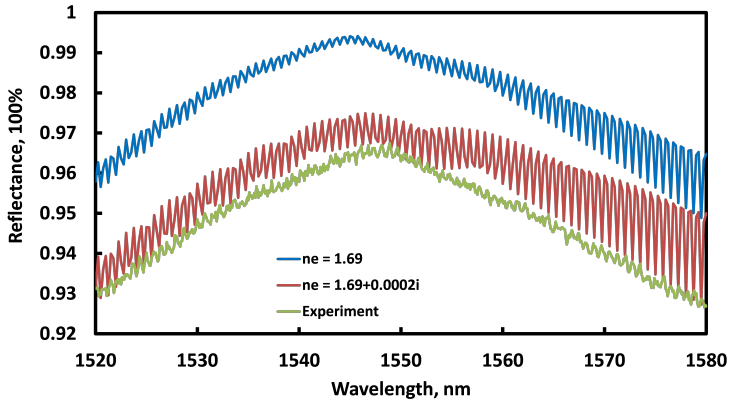

Figure 3. Combined (FEM and TMM) simulation and experimental results for the assembled LCOS panel.

3. PERFORMANCE EVALUATION

3.1 Phase Stability Measurements

Here we have measured the phase stability of the implemented LCOS device using the digital driving scheme (pulse-code modulation).[14] Phase shift and phase flicker were measured and calculated for different addressed phase levels. The phase shift between phase levels was measured interferometrically by analyzing the relative position of the interference fringes. In the measurement setup the half of the LCOS panel (part A) displayed 0 phase value (black image) and remain the same during the measurement, while the other half (part B) changed gradually from zero to the maximum level image (white). The high frame rate camera was used to capture the interference pattern in order to get high resolution in time.

Since the phase shift is varied with respect to both time and addressed phase values, the fluctuation of the phase shift over the time in each phase level was plotted here by showing the maximum (green line) and the minimum (dark blue line) of the measured phase shift value. We also present the mean values of measured phase shift for each addressed phase level (red line). The mean value of the total measured phase shift is 2.463π. The Fig. 4(a) is showing uncalibrated (non-linearized) electro-optical response. As for the phase flicker evaluation, we take the peak to peak value (PPV) by subtracting minimum measured phase shift from maximum measured phase shift for each addressed phase level to see the worst case (purple line). We also use the standard deviation (SD) to see the average amount of the flicker value over time for each addressed phase level (light blue line). Both PPV and SD are close to 0 as shown in the Fig. 4(a). To give an impression of the overall flicker response among the phase levels, the mean value for PPV and SD is 0.018π (0.73 %) and 0.004π (0.16 %) respectively. Then, in Fig. 4(b), we have shown the data after linearization for 256 phase levels (8 bit signal). The phase shift for each phase level is shown as blue line and for the corresponding flicker for each phase level is shown as red line. The maximum phase shift and mean flicker value remain the same as 2.463π and 0.004π respectively after the linearization. This indicated that the phase flicker is pretty low and thus stable for telecommunication applications.[10]

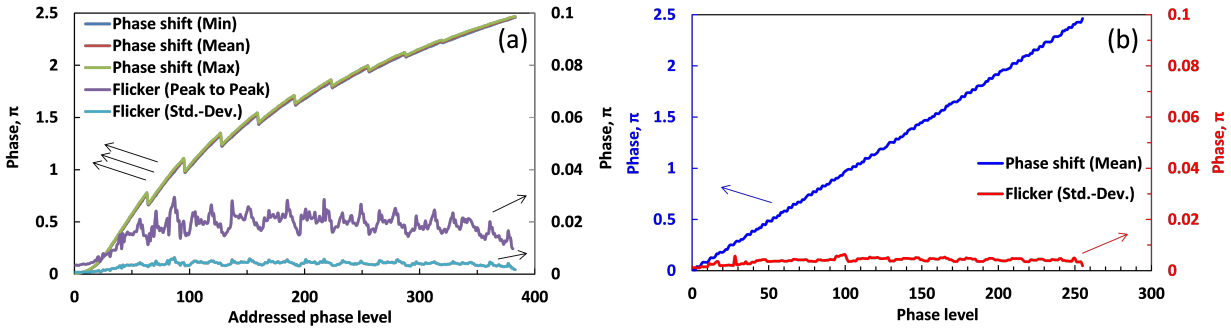

Figure 4. Phase stability measurement for the implemented LCOS panel and digital driving scheme before the linearization (a) and after the linearization (b).

3.2 Binary Grating Simulations and Measurements

With the experiment result showing low phase flicker over time, we now display the linear binary phase grating, where the period equals to 8 pixels, using the same driving scheme on the LCOS to see the optical performance at 1550 nm. The experiment result of horizontal binary grating and vertical grating is shown in Fig. 5(a) and (b), where the red squares and blue rhombs represent the simulation and experiment results of the diffraction efficiency for different diffraction orders. The horizontal grating means the grating lines are parallel to the alignment direction of LC (grating vector perpendicular to the alignment) while vertical grating means the opposite. The experiment results of the diffraction efficiency were achieved by varying the phase level of line part (higher phase shift) while maintaining the phase level as 0 for the groove part (lower phase shift) to find the minimum value of the 0^{th} order (reflection). The diffraction efficiency is first normalized to the reflected optical power of the gold mirror at 1550 nm then multiplied with the reflectance of gold mirror. As for the

simulation, theoretically,[15] the maximum diffraction efficiency for +/- 1^{st} order for the ideal binary grating with phase difference is 40.5 %. However, if we want to incorporate the twist effect, fringing field effect or material absorption into simulation, FEM simulation is needed. As a result, we take the calculated distribution of the LC director from LCD Master software (SHINTECH, INC) and import into the JCMsuite software to simulate the diffraction efficiency with FEM method.

For the horizontal grating, the measured diffraction efficiency is achieving around 35.3 % for the +/-1^{st} order. As for the vertical grating, we observed the $+1^{st}$ order and -1^{st} order diffraction efficiency are 39.6 % and 23.9 % respectively. We also observed diffraction efficiency were not equal to 0 in the even diffraction orders, which is due to the fringing field effect. Furthermore the experiment results differ between the horizontal and the vertical gratings. The difference of the energy distribution in diffraction orders between horizontal and vertical grating is due to the asymmetrical phase shift distribution that caused by the pretilt angle of LC molecules and the orientation relative to the alignment direction. As a result, even if we applied identical phase levels per period in both horizontal and vertical grating, the diffraction efficiency in +/-1^{st} order is not identical with each other. The FEM simulation results have predicted the influence due to the asymmetrical phase distribution and fringing field effect. The largest difference between the simulation and the experiment is in 0^{th} order. This is mainly due to the reflection from the ITO layer to the LC layer, where the original π phase difference between the pixels becomes 2π phase difference and contribute to the extra light leakage into the 0^{th} order. We also observed the diffraction efficiency for +/-1^{st} order in the simulation is slightly higher than in the experiment. This is expected since the cover glass was simulated with the infinite thickness by using the perfectly matched layer, thus the reflection loss at air-glass interface is neglected.

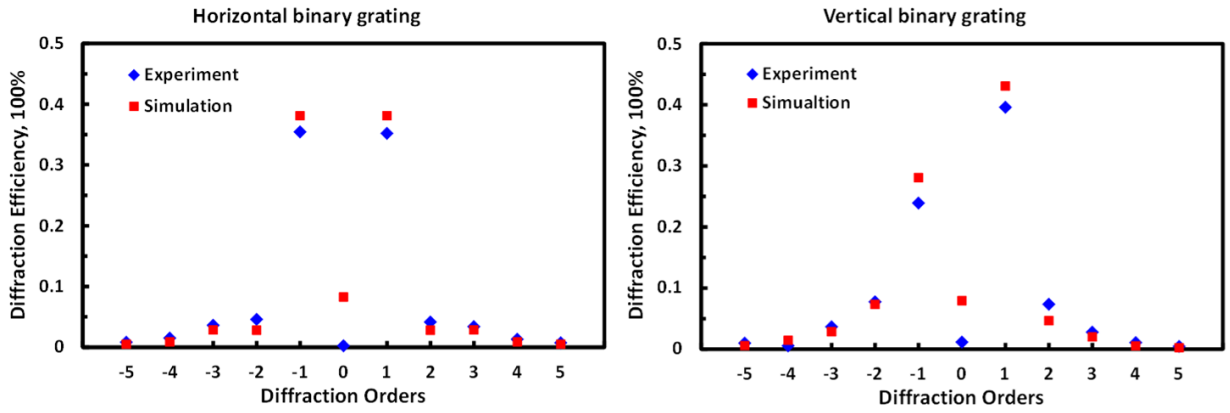

Figure 5. (a) Horizontal and (b) vertical binary grating simulation (red squares) and experiment results (blue rhombs).

3.3 Blazed Grating Simulations and Measurements

Here, we have shown the experiment and simulation results for the horizontal blazed grating with periods of 6 pixels in Fig. 6. In the experiment, the wavelength for the light source is again 1550 nm. The diffraction efficiency is normalized with respect to the gold mirror and then multiplied with the reflectance of gold mirror. By varying the slope of the phase distribution of the blazed grating, we found the maximum 1^{st} order diffraction efficiency is around -2.18 dB for the phase levels distributed as (255, 204, 153, 102, 51, 0) per period. Comparing to simulation results, where the 1^{st} order diffraction efficiency is -2.04 dB, we observed the experiment results is slightly lower. This is again due to the fact that the reflection loss in air-glass interface is not taken into consideration in the simulation. While for -2^{nd} to 0^{th} order, the experiments results are higher than the simulation results. The largest difference between the experiment and the simulation is in -2^{nd} diffraction order. The reason is mainly due to the reflection between the ITO layer and the LC layer. The diffracted light is propagating back again due to the reflection from ITO layer and experiencing again the diffraction on the blazed structure, thus contributes to the error in -2^{nd} order diffraction efficiency. This is also consistent with the fact that the simulation results for 0^{th} order in blazed grating are lower than that in binary grating. As for the errors in other orders, the

reason might be due to the 2D (not 3D) simulation, which neglects the fringing field effect in another direction. Finally, by using more pixels per period to make phase profile more linear, we can achieve higher diffraction efficiency for 1^{st} order. For example, the experiment results of 1^{st} order diffraction efficiency for 64 pixels and 16 pixels per period are -0.64 dB (∼86.4 %) and -1.21 dB (∼75.7 %). Those structures, however, are too large for the computation power we have now for simulation with FEM method.

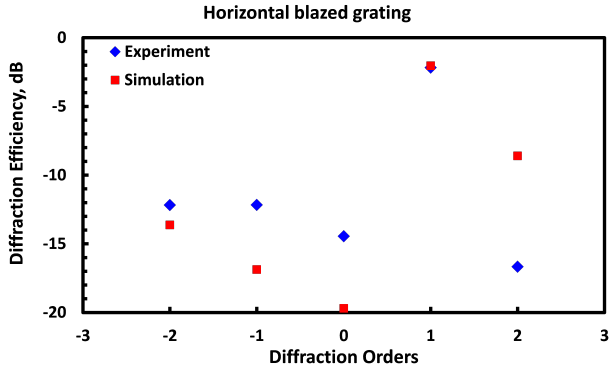

Figure 6. Horizontal blazed grating (period = 6 pixels) simulation (red squares) and experiment results (blue rhombs)

4. CONCLUSION

In conclusion, we have described the design principles for LCOS and reported the implementation of the high-reflectivity LCOS SLM for telecommunication applications. By comparing the simulation and experiment results for pixelated structure on the wafer with rigorous 3D FEM simulation methods, we have observed the reflectance in experiment is over 95.6% in both C- and L-band and the simulation has successfully predict the existence of resonance dip (reflectivity drop). Then, measurement and experiment results of the assembled LCOS panel with HRC layer have shown good reflectance for over 92.7 % to 96.7 % (IL between 0.15 dB and 0.33 dB) in both C- and L-band. Then, the phase shift measurement has shown the total phase shift 2.463π, where the phase flicker was low with SD = 0.004π. After the linearization two classical examples of diffractive optical element, binary grating and blazed grating, were evaluated and discussed. We have shown a promising optical performance, where 1^{st} order diffraction efficiency of the blazed grating have -0.64 dB (∼86.4 %) or -1.21 dB (∼75.7 %) using 64 pixels or 16 pixels per period, for telecommunication application.

ACKNOWLEDGMENTS

The authors would like to thank Xavier Garcia Santiago for helpful discussion and assistance in FEM simulation. This research was partially funded from the European Unions Horizon 2020 research and innovation program under the Marie Skłodowska-Curie Grant Agreements No. 675745 and 721465.

REFERENCES

[1] Lazarev, G., "Optimization of the liquid crystal on silicon technology for laser microprocessing applications," *Physics Procedia* **83**, 1153 – 1159 (2016).

[2] von Hoyningen-Huene, J., Ryf, R., and Winzer, P., "Lcos-based mode shaper for few-mode fiber," *Opt. Express* **21**(15), 18097–18110 (2013).

[3] Yang, D., He, C., Jing, Z., and Luo, F., "Research of two-dimensional beam steering in lcos-based wavelength selective switch," *Appl. Opt.* **54**(14), 4411–4416 (2015).

[4] Koebele, C., Salsi, M., Sperti, D., Tran, P., Brindel, P., Mardoyan, H., Bigo, S., Boutin, A., Verluise, F., Sillard, P., Astruc, M., Provost, L., Cerou, F., and Charlet, G., "Two mode transmission at 2x100gb/s, over 40km-long prototype few-mode fiber, using lcos-based programmable mode multiplexer and demultiplexer," *Opt. Express* **19**(17), 16593–16600 (2011).

[5] Salsi, M., Koebele, C., Sperti, D., Tran, P., Mardoyan, H., Brindel, P., Bigo, S., Boutin, A., Verluise, F., Sillard, P., Astruc, M., Provost, L., and Charlet, G., "Mode-division multiplexing of 2×100 gb/s channels using an lcos-based spatial modulator," *Journal of Lightwave Technology* **30**(4), 618–623 (2012).

[6] Baxter, G., Frisken, S., Abakoumov, D., Zhou, H., Clarke, I., Bartos, A., and Poole, S., "Highly programmable wavelength selective switch based on liquid crystal on silicon switching elements," in [*2006 Optical Fiber Communication Conference and the National Fiber Optic Engineers Conference*], 3 pp.– (2006).

[7] Frisken, S., Baxter, G., Abakoumov, D., Zhou, H., Clarke, I., and Poole, S., "Flexible and grid-less wavelength selective switch using lcos technology," in [*2011 Optical Fiber Communication Conference and Exposition and the National Fiber Optic Engineers Conference*], 1–3 (2011).

[8] Yamaguchi, K., Ikuma, Y., Nakajima, M., Suzuki, K., Itoh, M., and Hashimoto, T., "M×n wavelength selective switches using beam splitting by space light modulators," *IEEE Photonics Journal* **8**(2), 1–9 (2016).

[9] Xie, D., Wang, D., Zhang, M., Liu, Z., You, Q., Yang, Q., and Yu, S., "Lcos-based wavelength-selective switch for future finer-grid elastic optical networks capable of all-optical wavelength conversion," *IEEE Photonics Journal* **9**(2), 1–12 (2017).

[10] Wang, M., Zong, L., Mao, L., Marquez, A., Ye, Y., Zhao, H., and Vaquero Caballero, F. J., "Lcos slm study and its application in wavelength selective switch," *Photonics* **4**(2) (2017).

[11] Lazarev, G., Kerbstadt, F., and Luberek, J., "High-resolution high-reflective lcos spatial light modulator for beam manipulation beyond visible spectrum," *Proc.SPIE* **10090**, 10090 – 10090 – 6 (2017).

[12] Demkowicz, L., [*Computing with hp-ADAPTIVE FINITE ELEMENTS: Volume 1 One and Two Dimensional Elliptic and Maxwell Problems*], Chapman and Hall/CRC, Boca Raton (2007).

[13] Katsidis, C. C. and Siapkas, D. I., "General transfer-matrix method for optical multilayer systems with coherent, partially coherent, and incoherent interference," *Appl. Opt.* **41**(19), 3978–3987 (2002).

[14] Lazarev, G., Hermerschmidt, A., Kruger, S., and Osten, S., [*Optical Imaging and Metrology: Advanced Technologies*], John Wiley & Sons, Inc., Hoboken, NJ, USA (August 2012).

[15] Lu, T., Pivnenko, M., Robertson, B., and Chu, D., "Pixel-level fringing-effect model to describe the phase profile and diffraction efficiency of a liquid crystal on silicon device," *Appl. Opt.* **54**(19), 5903–5910 (2015).